Analytica Chimica Acta 883 (2015) 81–89

Contents lists available at ScienceDirect

Analytica Chimica Acta

journal homepage: www.elsevier.com/locate/aca

Aptamer-functionalized nanoporous gold film for high-performance direct electrochemical detection of bisphenol A in human serum

Ye Zhu [a,*], Chuqing Zhou [a], Xupeng Yan [a], Yan Yan [a], Qiang Wang [b,*]

[a] School of Chemistry and Chemical Engineering, Shandong University, Jinan 250100, China
[b] Institute of New Energy Materials & Low-Carbon Technologies, Tianjin University of Technology, Tianjin 300384, China

HIGHLIGHTS

- NPGF exhibits excellent catalytic activity towards the redox reaction of BPA.
- The perfect combination of NPGF with aptamer ensures high sensitivity and selectivity.
- The detection limit is determined to be 0.056 ± 0.004 nM BPA.
- The detection limit is 15-fold lower than gold nanoparticle-based sensor.
- The sensor was successfully applied to detect BPA in human serum samples.

GRAPHICAL ABSTRACT

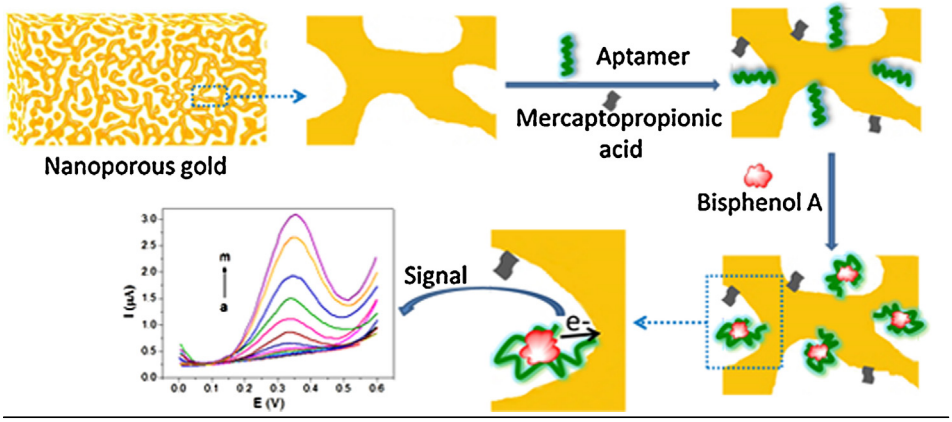

ARTICLE INFO

Article history:
Received 4 March 2015
Received in revised form 28 April 2015
Accepted 2 May 2015
Available online 6 May 2015

Keywords:
Nanoporous gold
Aptamer sensor
Bisphenol A
Direct electrochemical detection
Electrocatalysis

ABSTRACT

In the present work, a highly sensitive and selective biosensor based on aptamer-functionalized nanoporous gold film (NPGF) was successfully developed for direct electrochemical detection of bisphenol A (BPA). NPGF was prepared by dealloying Ag from Au/Ag alloy leaf in concentrated nitric acid. The obtained NPGF was attached onto glassy carbon electrode and then was functionalized with BPA-specific aptamer via the formation of Au—S bond. The fabrication of the sensor was characterized by scanning electron microscopy and X-ray photoelectron spectroscopy. NPGF exhibited excellent electrocatalytic activity towards the redox reaction of BPA, which ensured high sensitivity of the sensor. The aptamer-captured BPA showed a pair of redox peaks around 0.35/0.28 V (vs. Ag/AgCl). The experimental parameters in terms of aptamer concentration, reaction time, pH, and temperature were optimized. The calibration plot showed a linear range from 0.1 nM to 100 nM BPA with a remarkable detection limit of 0.056 ± 0.004 nM BPA. Particularly, the successful application of the developed sensor for the detection of BPA in human serum samples suggests its promising potential for clinical diagnosis.

1. Introduction

Bisphenol A (BPA) is an important chemical monomer for the synthesis of polycarbonate polymers and epoxy resin, which are widely used as food-storage and packaging materials such as feeding bottles, water bottles, tableware, and the inner coating of

* Corresponding author. Tel.: +86 531 88363089; fax: +86 531 88363089.
E-mail addresses: zhuye@sdu.edu.cn (Y. Zhu), qiangwang@tjut.edu.cn (Q. Wang).

http://dx.doi.org/10.1016/j.aca.2015.05.002
0003-2670/

cans. The widespread use of BPA and its permeation into food and environment from the storage and packaging materials lead to growing concerns about human health [1–3], because BPA is one of potent endocrine-disrupting compounds [3] which can mimic the action of hormone estrogen and disturb the estrogen–estrogen receptor binding process thereby being monitored by various techniques including gas chromatography [4], surface-enhanced Raman scattering [5], and so on [6]. Besides disturbing the human endocrine system, BPA is also associated with obesity, neurotoxicity, and even cancer [7,8]. Therefore, development of analytical methods for BPA detection is an urgent undertaking. Up to date, many methods have been developed for the detection of BPA in simple matrices, such as water, however, monitoring BPA in human internal fluids has rarely been explored due to the matrix effect of the biological samples [9]. Obviously, the latter is of critical importance for evaluating and controlling the harmful effects of BPA on human health. Therefore, development of highly sensitive, selective, and reliable methods for trace level determination of BPA in human internal fluids is extremely desirable.

A number of analytical methods for the detection of BPA have been developed, most of which are chromatography and mass spectrometry-based techniques [10]. These chromatography and mass spectrometry-based techniques can analyze BPA with high sensitivity, however, large capital investment, skilled operators, and cumbersome sample preparation and pretreatment are required, reducing their applicability of on-site and rapid detection of BPA in various samples and matrices [9,11]. The other recently developed methods for BPA detection include enzyme-linked immunosorbent assay (ELISA) [12], fluorescent method [13], surface-enhanced Raman scattering [14,15], colorimetric methods [16], and electrochemical sensors [17–29]. Among those methods, electrochemical sensors are the widely accepted and employed group due to their simple operation, rapid response time, low cost, high sensitivity, potential for miniaturization, and capability of real sample analysis [9], thereby having promising potential for BPA analysis in human internal fluids. Furthermore, since BPA is electroactive due to its phenolic groups, direct electrochemical detection of BPA without a label can facilitate the sensor fabrication and detection process. To enhance the detectable signals, nanomaterials that possess large specific surface area and electrocatalytic property are usually utilized to catalyze the redox reaction of BPA. Electrochemical sensors that were developed with metal nanoparticles [18], quantum dots [19], carbon nanotubes [20,21], graphene [17,22–24], and the composite of nanomaterials [25–27] have been reported for the detection of BPA. Besides BPA, however, there are many other phenolic compounds that also can be electrocatalyzed by the nanomaterials mentioned above, which may interfere the detection of BPA. To improve the selectivity of the sensors for BPA detection, biomolecules including antibodies [28], aptamers [26,29,30], peptides [17,31], and estrogen receptors [32] have been used as recognizers. Ragavan et al. pointed out that simpleness, high sensitivity, high selectivity, and the capability for detecting BPA in complex matrices are the developing trends of BPA sensors and nanotechnology is the one of the likely areas to show encouraging prospects for developing sensors for detection of BPA by overcoming the shortcomings of currently-available analytical procedures [9]. Therefore, the nanomaterials combining excellent electrocatalytic properties with good biocompatibility is worth to explore for the development of BPA sensors.

Nanoporous gold film (NPGF) that is prepared by dealloying method has been attracting wide interests since it was reported in 2004 [33]. It is bicontinuous nanoporous with both the void space and the scaffold completely interconnected, mechanical rigid, chemical stable, highly conductive, and biocompatible. Its excellent catalytic properties and optical properties have been widely utilized for various purposes [34,35]. It also exhibits excellent electrocatalytic property towards small molecular chemicals [36,37]. However, combination of the excellent electrocatalytic properties of NPGF with specific biomolecular recognizers for highly sensitive and selective electrochemical biosensors has not been explored well. Taking the advantages of NPGF into consideration, it must be a kind of promising material for the development of electrochemical biosensors for BPA detection in complex matrices.

In the present work, a novel biosensor based on aptamer-functionalized NPGF was developed for direct electrochemical detection of BPA. NPGF was prepared by dealloying Ag from Au/Ag alloy leaves in concentrated nitric acid and was attached onto glassy carbon electrode (GCE). Then, the NPGF modified GCE was functionalized with BPA-specific aptamer via the formation of Au-S bond. The fabricated aptamer/NPGF/GCE sensor was characterized by scanning electron microscope (SEM) and X-ray photoelectron spectroscopy (XPS). The electrochemical catalytic property of NPGF towards the redox reaction of BPA was comprehensively studied by cyclic voltammetry (CV). The experimental parameters in terms of aptamer concentration, reaction time, pH, and temperature were optimized. The detection of BPA in phosphate buffer solution (PBS) and human serum sample with the developed sensor was achieved by differential pulse voltammetry (DPV).

2. Materials and methods

2.1. Chemicals and materials

BPA was purchased from Aladdin Industrial Corporation (Shanghai, China). A 5′-thiolated DNA aptamer (5′-CCG GTG GGT GGT CAG GTG GGA TAG CGT TCC GCG TAT GGC CCA GCG CAT CAC GGG TTC GCA CCA-3′) that is specific to BPA [38] was synthesized by Invitrogen Biotechnology Co., Ltd. (Beijing, China). Human serum sample was collected from healthy people. PBS was prepared with 0.01 M disodium hydrogen phosphate, 0.01 M sodium dihydrogen phosphate, and 0.9% sodium chloride. TE buffer (pH 8.0) prepared with 10 mM tris(hydroxymethyl) aminomethane and 1 mM ethylenediaminetetraacetic acid was used to dilute aptamer. All other chemicals were of extra pure analytical grade and were used without further purification. Au/Ag alloy leaves (100 nm in thickness; 50:50, w/w) were purchased from Changshu Noble Metal Company (Changshu, China). Ultra-pure water with resistance of 18.25 MΩ cm was used to prepare all aqueous solutions.

2.2. Apparatus

The electrochemical experiments were conducted with a three-electrode system, including the modified GCE (area 0.07 cm^2), Ag/AgCl (in saturated KCl), and a platinum wire as the working, reference, and counter electrode, respectively. CV and DPV were performed on a CHI 660E Electrochemical Workstation (Shanghai Chenhua, China). The morphology of NPG was characterized by a Hitachi S-4800 ultrahigh resolution (UHR) field emission (FE) scanning electron microscope, at an accelerating voltage of 5.0 kV. XPS experiments were carried out using a monochromatized XPS spectrometer (Thermo Fisher ESCALAB 250) with Al (Kα) radiation as the probe and 500 μm analysis spot size. Electrochemical impedance spectroscopy (EIS) was recorded with PARSTAT 2263 with frequency scanning from 100 Hz to 1 MHz at the open circuit voltage.

2.3. Preparation of NPGF

NPGF was prepared by dealloying of Ag from Au/Ag alloy leaves [33]. Briefly, Au/Ag alloy leaves were cut into small pieces (8 mm × 8 mm) and etched in concentrated nitric acid at 30 °C for 30 min. As a result, the leaves changed into golden color from

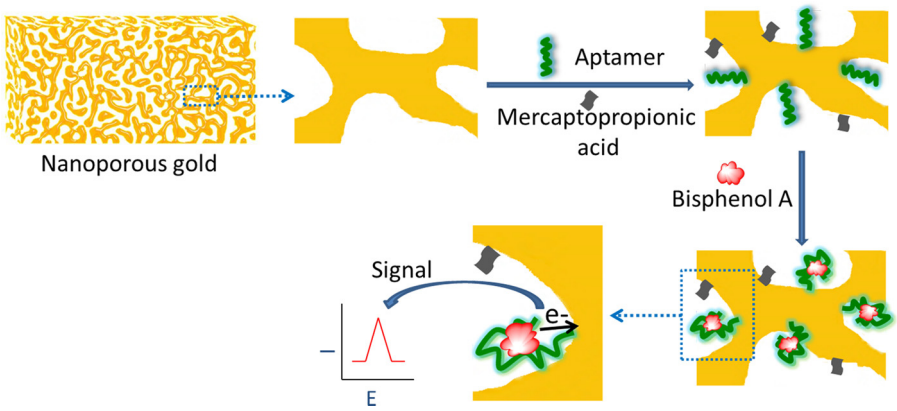

Scheme 1. Schematic representation of the NPGF-based aptamer sensor for direct electrochemical detection of BPA.

silver-white color because of the removal of Ag from the Au/Ag alloy, and NPGF was obtained. After washing thoroughly with ultra-pure water three times, the obtained NPGF floated on ultra-pure water for further use.

2.4. Fabrication of aptamer/NPGF/GCE

Firstly, GCE was polished to a mirror finish using alumina slurry (0.3 μm and 0.05 μm, respectively) on chamois leather, followed by ultrasonic cleaning for 15 s to remove the alumina particles and other impurities before rinsing by ultra-pure water and ethanol successively. Then, the previously prepared NPGF floating on ultra-pure water was fished out by the prepared GCE. After drying for 24 h, NPGF was firmly attached onto the GCE surface through physical adsorption. After that, the part of the NPGF covering outside of GCE was carefully removed by a stick, keeping the area of NPGF same as that of the GCE (0.07 cm^2). Then, BPA-specific aptamer modified with —SH group at terminal was drop coated onto the obtained NPGF/GCE and subsequently incubated at 4 °C overnight. Consequently, the aptamer was immobilized onto the ligament of NPGF through the formation of S—Au bond, as illustrated in Scheme 1. After washing with TE buffer to remove the unbound aptamer, 1 mM mercaptopropionic acid was dropped onto the aptamer-immobilized NPGF/GCE and incubated for 30 min to reduce the unspecific adsorption. Finally, the fabricated aptamer/NPGF/GCE sensor was washed with TE buffer and stored in refrigerator at 4 °C for further use.

2.5. Detection of BPA with the aptamer/NPGF/GCE sensor

To detect BPA, the fabricated aptamer/NPGF/GCE sensor was immersed into 0.1 M PBS (pH 7.5) containing BPA for 30 min. After incubation, the sensor was washed with 0.1 M PBS and measured in 0.1 M PBS (pH 7.5) with a three-electrode system. Then, CVs and DPVs were recorded to study the NPGF-electrocatalyzed redox reaction of the captured BPA, as illustrated in Scheme 1.

2.6. Detection of BPA in human serum samples

The human serum sample was collected from healthy people. At the beginning, the serum sample was centrifuged at 10,000 rpm for 5 min. The resulting supernate was diluted five times with 0.1 M PBS (pH 7.5). Afterwards, 100 μL of BPA standard solution (containing 5, 10, 50, 100, and 500 nM BPA, respectively) prepared with 0.1 M PBS (pH 7.5) was spiked into 1 mL of the diluted serum sample, making the final concentrations of 0.5, 1.0, 5.0, 10, and 50 nM BPA, respectively. Then, the fabricated aptamer/NPGF/GCE sensor was immersed into the BPA-spiked serum samples for 30 min, followed by washing with 0.1 M PBS (pH 7.5). Finally, DPVs were recorded in 0.1 M PBS to evaluate the BPA concentration in the diluted serum samples.

3. Results and discussion

3.1. Catalytic property of NPGF towards BPA

Before fabrication of the aptamer/NPGF/GCE sensor, the catalytic property of NPGF towards BPA was firstly studied by using NPGF/GCE as a working electrode. The recorded CV in 0.1 M PBS (pH 7.5) containing 200 μM BPA showed a significant oxidation peak at 0.43 V (curve a in Fig. 1A), which was consistent with the previously reported oxidation potential of BPA by using other electrodes [39,40]. In contrast, the CV recorded for NPGF/GCE in 0.1 M PBS (pH 7.5) without BPA did not show any peak (curve d in

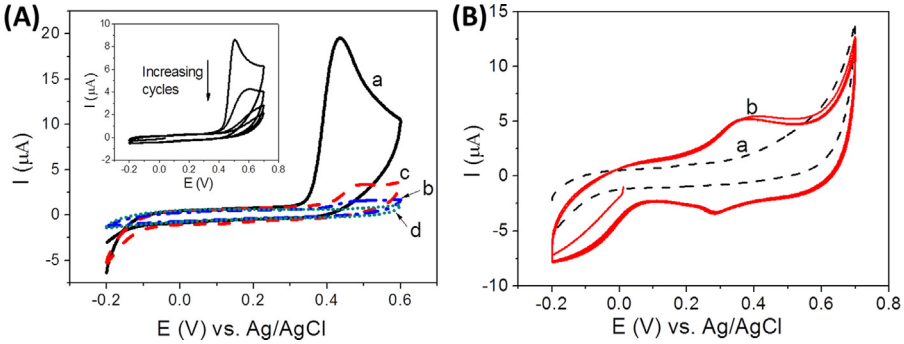

Fig. 1. (A) CVs of (a) NPGF/GCE, (b) GCE, and (c) bulk gold disk electrode in 0.1 M PBS containing 200.0 μM BPA, and (d) CV of NPGF/GCE in 0.1 M PBS, inset shows the multiple CVs of NPGF/GCE in 0.1 M PBS containing 50.0 μM BPA; (B) CVs of (a) aptamer/NPGF/GCE and (b) BPA/aptamer/NPGF/GCE in 0.1 M PBS.

Fig. 1A), indicating that the obtained oxidation peak in curve a belongs to BPA. To further evaluate the catalytic property of NPGF, control experiments were conducted by using bare GCE and bulk gold disk electrode as a working electrode, respectively. The obtained CVs for both GCE and bulk gold disk electrode in 0.1 M PBS (pH 7.5) containing 200 μM BPA exhibited the oxidation peak of BPA around 0.5 V (curve b and c in Fig. 1A). Obviously, the BPA oxidation peak by using NPGF/GCE showed lower overpotential compared with that obtained for GCE and bulk gold disk electrode. Moreover, the intensity of the peak current for NPGF/GCE was 23-fold and 9-fold higher than that for GCE and bulk gold disk electrode, respectively, indicating excellent catalytic property of NPGF towards BPA. According to this result, high sensitivity of NPGF-based aptamer sensor for BPA detection is expected.

Continuous sweeping of potential was performed in 0.1 M PBS (pH 7.5) containing 50 μM BPA by using NPGF/GCE. The recorded CVs exhibited decreasing oxidation peak currents with the increasing cycles (inset of Fig. 1A), which was similar to the previous report [39]. This phenomenon was resulted from the electropolymerization of the BPA onto NPGF surface from bulk solution, which was demonstrated with SEM (Fig. S1 in Supporting information). Thereby poly-BPA occupied the catalytic active sites and gradually reduced the catalytic property of NPGF towards BPA. However, it was worthwhile to note that such phenomenon was not observed when BPA was detected by aptamer/NPGF/GCE sensor (Fig. 1B), which would be discussed in Section 3.3.

3.2. Characterization of aptamer/NPGF/BPA

The fabrication of the aptamer/NPGF/GCE sensor was characterized by SEM. NPGF exhibited a three dimensional structure with a pore size in a range of 30–50 nm which was similar with the ligament size (Fig. 2A). After immobilization of aptamer, the observed image became 'more crowed' (Fig. 2B) compared with that of NPGF. Moreover, at a high resolution, clean ligament surface of NPGF was observed (Fig. 2C), while a thin layer was observed on the ligament surface of NPGF after immobilization of aptamer (Fig. 2D).

To further demonstrate the immobilization of aptamer, the prepared sensor was characterized by XPS. The XPS spectra for NPGF/GCE and aptamer/NPGF/GCE were calibrated using C 1s peak at 284.6 eV as an internal standard, as shown in Fig. 2E. The C 1s peak revealed at 284.6 eV due to the C—C and C—H bonds, and a common O 1s peak was observed at 532.1 eV for all surfaces. Two Au 4f peaks were observed at 86.2 eV and 83.6 eV for all surfaces. Compared with the spectrum for NPGF/GCE, the P 2p peak was observed for aptamer/NPGF/GCE at 131.9 eV, which corresponded to phosphate, the major structural components of aptamer backbone [41]. Furthermore, the N 1s peak was observed for aptamer/NPGF/GCE at 400.0 eV due to the C—N bond contained in DNA bases, which was a reliable indication for that the aptamer was successfully immobilized on the NPGF surface [42]. Based on the specific spectra of Au 4f and N 1s (Fig. S2 in Supporting information), the atom ratio of Au:N was calculated to be 89.1:10.9. Combining with the horizontal projected area of gold atom (2.27×10^{-20} m^2) and the number of nitrogen atom in each aptamer molecule (243 N atoms), the surface coverage of the immobilized aptamer was calculated to be 3.68 pmol/cm^2, which was similar with the previously reported surface coverage of the immobilized DNA onto gold surface [42].

The fabrication of the aptamer/NPGF/GCE sensor was further characterized by EIS in 0.1 M KCl solution containing 5.0 mM $K_3[Fe(CN)_6]/K_4[Fe(CN)_6]$. The frequency was scanned from 100 Hz to 1 MHz at the open circuit voltage. The obtained Nyquist plots for GCE (a), NPGF/GCE (b), and aptamer/NPGF/GCE (c) are presented in Fig. 2F. A well defined semicircle at high frequencies was observed for all the electrodes. A general circuit (inset of Fig. 2F) was utilized to fit the impedance data for the present system, where R_s represents solution resistance, R_{et} is the electron transfer resistance, W is the Warburg element, and CPE is the constant phase element. The fitting value of R_{et} for bare GCE was about 895 Ω. After modification with NPGF, a smaller semicircle

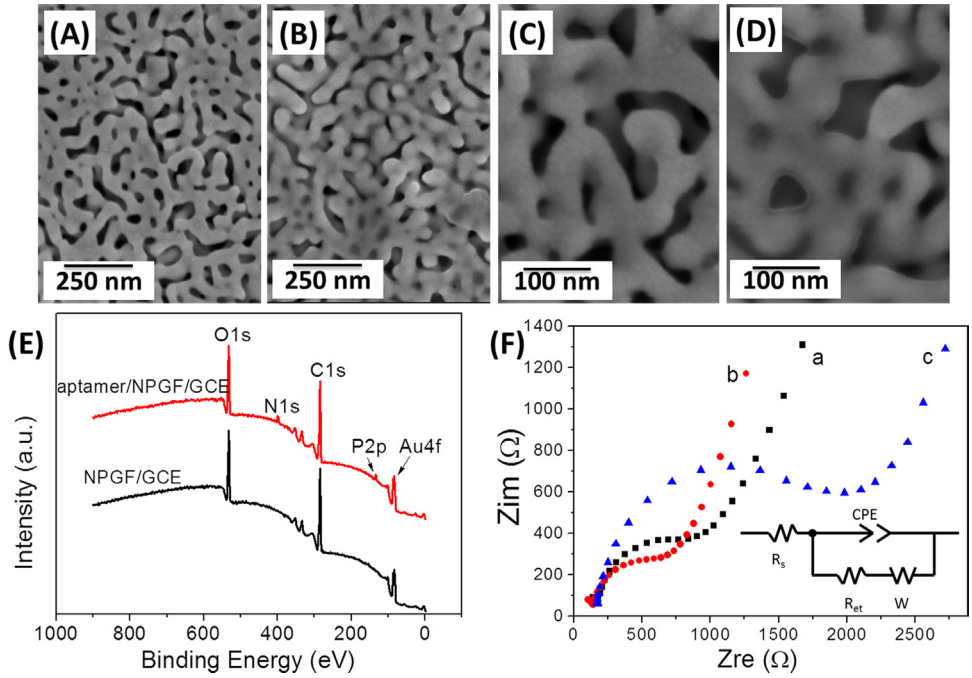

Fig. 2. SEM images of NPGF (A and C) and aptamer/NPGF (B and D); (E) XPS survey spectra for NPGF/GCE and aptamer/NPGF/GCE; (F) Nyquist plots for (a) GCE, (b) NPGF/GCE, and (c) aptamer/NPGF/GCE in 0.1 M KCl solution containing 5.0 mM $K_3[Fe(CN)_6]/K_4[Fe(CN)_6]$.

was observed and the fitting value of R_{et} decreased to 546 Ω, indicating the improved conductivity of the electrode because of the modification of NPGF. Aptamer/NPGF/GCE exhibited a large semicircle with an increased R_{et} value of 1826 Ω, which was attributed to the electrostatic repulsion between the negatively charged aptamer and $Fe(CN)_6^{3-}/Fe(CN)_6^{4-}$. The EIS characterization further demonstrated the successful fabrication of the aptamer/NPGF/GCE sensor.

3.3. Electrochemical behavior of BPA on aptamer/NPGF/BPA sensor

The electrochemical behavior of BPA that was captured by aptamer/NPGF/GCE sensor was studied with CV in a three-electrode system. As a blank experiment, CV for the aptamer/NPGF/GCE in 0.1 M PBS (pH 7.5) was firstly recorded and no redox peak was observed (curve a in Fig. 1B). Then, the aptamer/NPGF/GCE sensor was incubated with 50 μM BPA in 0.1 M PBS (pH 7.5), where the aptamer could recognize and capture BPA. After washing with 0.1 M PBS to remove the unbound BPA, the obtained BPA/aptamer/NPGF/GCE was tested in 0.1 M PBS (pH 7.5). The recorded curve b (in Fig. 1B) exhibited a pair of redox peaks around 0.35/0.28 V, which corresponded to the redox reaction of BPA that was captured by the aptamer on the sensor. Interestingly, the electrochemical behavior of aptamer-captured BPA was different from that of free BPA in solution phase which only exhibited an oxidation peak, as shown in Fig. 1A. Moreover, the multiple CVs for aptamer-captured BPA showed constant peak current (curve b in Fig. 1B), while the oxidation peak current of free BPA gradually decreased with the increasing cycles (inset of Fig. 1A). There are two reasons leading to these phenomena: first, the capture of BPA by aptamer immobilized on NPGF shortened the distance between BPA and NPGF, thereby facilitating the catalysis towards the redox reaction of BPA; second, one BPA molecule was captured by one aptamer molecule, avoiding the irreversible polymerization of BPA molecules that happened towards BPA in bulk solution (Fig. S1 in Supporting information).

To infer the electrochemical reaction mechanism of BPA captured by aptamer/NPGF/GCE, the effect of scan rate on BPA redox reaction was investigated. The obtained CV responses of BPA/aptamer/NPGF/GCE in 0.1 M PBS at varying scan rate are shown in Fig. 3A. As the scan rate was increased from 20 to 200 mV s^{-1}, the redox peak current gradually increased. Both the anodic current and the cathodic peak current were proportional to the applied scan rate (Fig. 3B), indicating that the electrochemical reaction is a typical adsorption-controlled process. This result also indicates the successful recognition and capture of BPA by the aptamer sensor. According to the electrochemical responses of adsorbed electroactive species [43,44], there are,

$$\Delta E_{pc,1/2} = \frac{62.5}{\alpha n}\text{mV} \quad (1)$$

$$\Delta E_{pa,1/2} = \frac{62.5}{(1-\alpha)n}\text{mV} \quad (2)$$

where $\Delta E_{pa,1/2}$ and $\Delta E_{pc,1/2}$ are the width at half-height of the anodic peak and the cathodic peak, respectively; α is the electron transfer coefficient; and n is the electron transfer number. Based on the CV at 200 mV s^{-1} in Fig 3A, $\Delta E_{pa,1/2}$ and $\Delta E_{pc,1/2}$ were determined to be 173.4 mV and 81 mV, respectively. Then, the values of α and n were calculated to be 0.68 and 1.1, respectively. Therefore, the electron transfer number for the redox reaction of aptamer-captured BPA was determined to be 1. Furthermore, the effect of the pH of the electrolyte solution on BPA redox reaction was also investigated in 0.1 M PBS with the pH values varying from 5.5 to 7.8. The redox reaction peak of the aptamer-captured BPA shifted negatively with the increasing pH value. The linear relationship between the formal potential of BPA redox reaction ($E^{0'}$, the average value of the oxidation potential and the reduction potential) and the pH could be expressed as: $E^{0'}$ (V) = −0.0656 pH + 0.8889 with a correlation coefficient of 0.993, as shown in Fig. 3C. The slope of 65.6 mV pH^{-1} suggests that the number of transferred electrons and protons

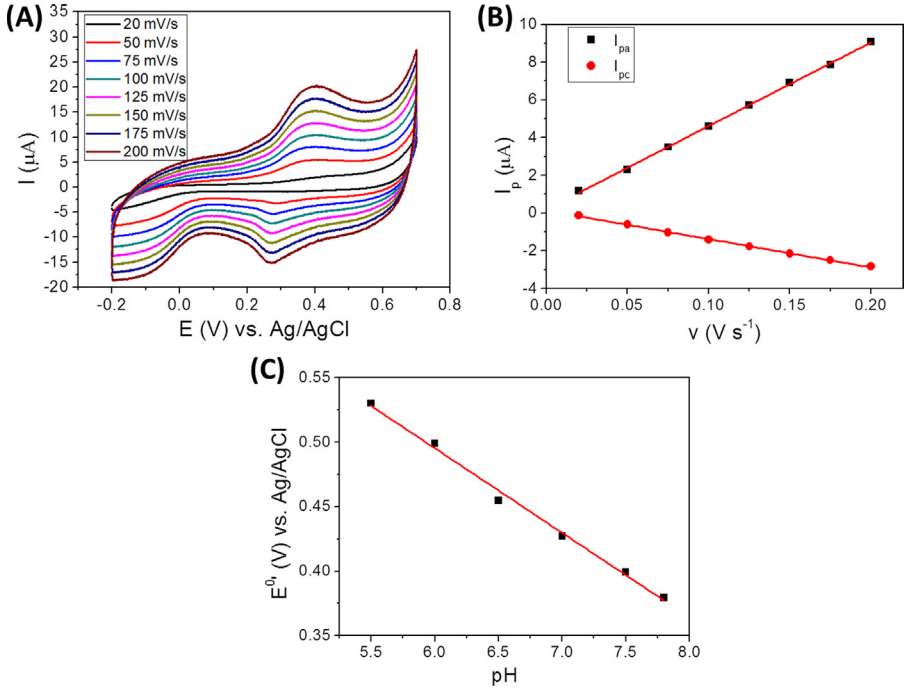

Fig. 3. (A) CVs of BPA/aptamer/NPGF/GCE in 0.1 M PBS at varying scan rates; (B) the linear relationship between peak current and scan rate; (C) the linear relationship between the formal potential of aptamer-captured BPA redox reaction and the pH of the electrolyte solution.

involved in the electrochemical redox reaction process is equal [43]. Therefore, we can infer that the electrochemical redox reaction of the aptamer-captured BPA is a one-electron and one-proton process. The electrochemical reaction mechanism of the aptamer-captured BPA can be inferred as below,

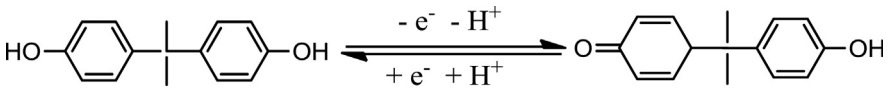

There is only one phenolic group involved in the electrochemical redox reaction. The other one is probably stabilized by the binding of the aptamer, thereby avoiding being oxidized easily.

3.4. Optimization of the experimental conditions

To achieve the best performance of the developed sensor, the experimental parameters were optimized in terms of aptamer concentration, reaction time, pH, and temperature. The effect of capturing aptamer concentration on the sensor response was investigated by drop coating different concentrations (0.1, 0.5, 1.0, 2.0, 5.0, 8.0, 10.0, 12.0 μM) of aptamer onto the surface of NPGF/GCE. After incubation overnight and blocking with mercaptopropionic acid, the obtained aptamer/NPGF/GCE reacted with 50 μM BPA in 0.1 M PBS (pH 7.5). Then, DPVs were recorded to evaluate the aptamer concentration effect on the sensor response. As shown in Fig. 4A, the current response significantly increased with increasing aptamer concentrations at low concentration range. However, there was no significant increase in the response for the concentration of aptamer above 5.0 μM, due to the saturation of the active sites for aptamer immobilization. Thus, an aptamer concentration of 5.0 μM was used for sensor fabrication.

To investigate the effect of reaction time with respect to BPA uptake, the aptamer/NPGF/GCE sensor was immersed in 0.1 M PBS (pH 7.5) containing 50 μM BPA for different time interval (0–35 min) and the DPVs were recorded for the captured BPA. The relationship between the sensor response and the reaction time is shown in Fig. 4B. The response appeared after 3 min, and then gradually increased with increasing reaction time. Because of the three-dimensional structure of NPGF, the delivery of BPA molecules towards the aptamers that were immobilized internal pore of NPGF was controlled by diffusion, thereby leading to extended reaction time. After 30 min, there was no significant increase in the peak current observed due to the saturation of the binding sites for BPA. Thus, 30 min was selected as the adequate reaction time for the aptamer/NPGF/GCE sensor to interact with BPA.

Further, the effect of pH on the sensor response was evaluated by recording DPVs for the BPA-captured probe in 0.1 M PBS with varied pH values from 5.5 to 8.0. The current increased as the medium pH increased from 5.5 to 7.5 and then decreased at the pH values higher than 7.5 (Fig. 4C). The maximum current was observed at a pH of 7.5, so all subsequent experiments were performed in 0.1 M PBS of pH 7.5.

In addition, the effect of test temperature on the current response was investigated between 15 °C and 50 °C. The peak current increased significantly as the temperature increased from 15 °C to 40 °C and then suddenly decreased over 40 °C, as shown in Fig. 4D. The decrease of the sensor response over 40 °C might be due to the thermal change of the NPGF structure at the elevated temperature. Taking the thermal stability of NPGF into consideration, 30 °C was selected as the optimal temperature.

3.5. Detection of BPA

Under the above optimal experimental conditions, the aptamer/NPGF/GCE sensor was used to detect varying concentrations of BPA (0–150.0 nM) in 0.1 M PBS. The recorded DPVs are exhibited in Fig. 5A (inset shows the enlarged DPVs for BPA at low concentrations (0–5.0 nM)), which showed a gradual increase in current with the increasing BPA concentration. The corresponding calibration curve exhibited a good linearity from 0.1 nM to 100 nM BPA (curve a in Fig. 5B, inset shows the enlarged calibration plots of the aptamer/NPGF/GCE sensor at low BPA concentrations (0–5.0 nM)). The linear dependencies of BPA analysis yielded an equation, I_p (μA) = (0.045 ± 0.002) + (0.017 ± 0.0003) [BPA] (nM) with a correlation coefficient of 0.997. The sensitivity of the aptamer sensor was 0.017 ± 0.0003 μA nM^{-1}. Based on five measurements for the standard deviation of the blank noise (95% confidence level, k = 3, n = 5), the detection limit was determined to be 0.056 ± 0.004 nM BPA. The linear range and the detection limit of the developed sensor were compared with several previously reported electrochemical sensors for BPA detection, as exhibited in Table 1. We can see that the developed sensor shows a lower detection limit than most of those works.

In addition, to further demonstrate the catalytic property of NPGF and evaluate the performance of the developed aptamer/NPGF/GCE sensor, control experiments were conducted by using gold nanoparticle (AuNP)-based aptamer sensor for BPA detection.

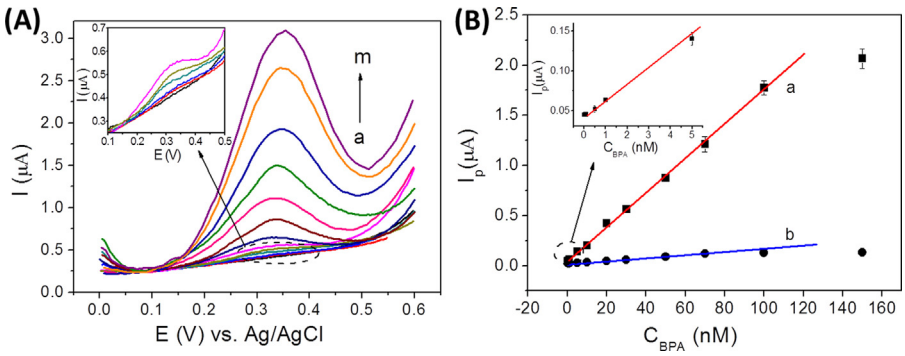

Fig. 5. (A) DPV responses of the aptamer/NPGF/GCE sensor to varying concentrations of BPA (from a to m: 0, 0.05, 0.1, 0.5, 1.0, 5.0, 10.0, 20.0, 30.0, 50.0, 70.0, 100.0, 150.0 nM), inset shows the enlarged DPVs for BPA at low concentrations (0–5.0 nM); (B) calibration plots of (a) the aptamer/NPGF/GCE sensor and (b) the aptamer/AuNPs/GCE sensor to BPA concentrations, inset shows the enlarged calibration plots of the aptamer/NPGF/GCE sensor at low BPA concentrations (0–5.0 nM).

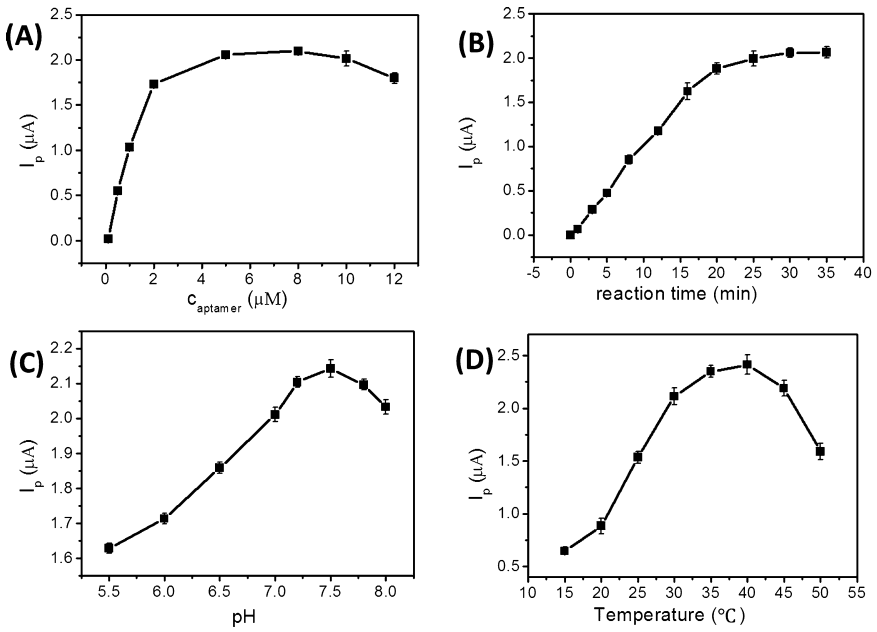

Fig. 4. Optimization of the experimental parameters: effects of (A) aptamer concentration, (B) reaction time, (C) pH, and (D) temperature on the sensor response.

The sensor was fabricated by electrochemically depositing AuNPs onto GCE followed by immobilization of BPA-specific aptamer onto AuNPs through S—Au bond. Using the fabricated aptamer/AuNPs/GCE sensor, detection of BPA with varying concentrations was carried out. The obtained calibration plots (curve b in Fig. 5B) yielded an equation of I_p (μA) = (0.0192 ± 0.0008) + (0.0014 ± 0.0001) [BPA] (nM) with a correlation coefficient of 0.996. The detection limit was calculated to be 0.82 ± 0.007 nM, which was about 15-fold higher than that of the developed aptamer/NPGF/GCE sensor. The low detection limit of the developed aptamer/NPGF/GCE sensor was attributed to the excellent catalytic property of NPGF towards the redox reaction of BPA and the bicontinuous three dimensional structure which could facilitate the electron transfer and molecule diffusion.

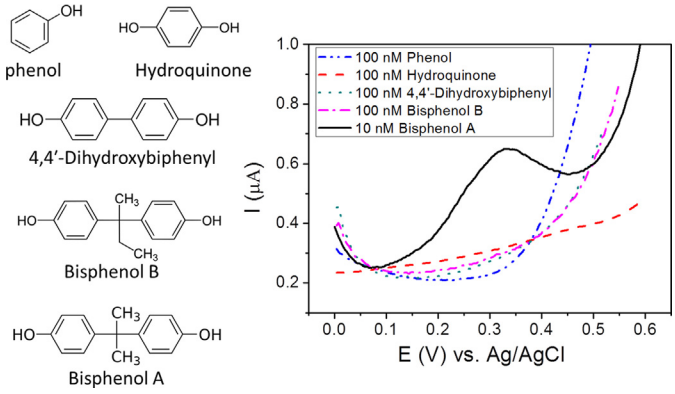

Fig. 6. DPV responses of the aptamer/NPGF/GCE sensor to different analytes.

Table 1
Comparison of several electrochemical sensors for BPA detection.

Modified electrodes	Methods	Linear range (M)	Detection limit (M)	References
G-MN202/chitosan/GCE	DPV	5.0×10^{-9}–2.0×10^{-5}	1.02×10^{-9}	[23]
N-GS/chitosan/GCE	Amperometry	1.0×10^{-8}–1.3×10^{-6}	5.0×10^{-9}	[24]
PGA/CNT/GCE	DPV	1.0×10^{-7}–1.0×10^{-5}	2.0×10^{-8}	[20]
Arg-G/GCE	DPV	5.0×10^{-9}–4.0×10^{-5}	1.0×10^{-9}	[22]
PPILF/GCE	DPV	1.0×10^{-8}–1.0×10^{-5}	8.0×10^{-9}	[40]
Fe_3O_4/carbon black/GCE	DPV	1.0×10^{-10}–5.0×10^{-5}	3.1×10^{-11}	[27]
rGO-Fc-NH_2/AuNPs/GCE	DPV	5.0×10^{-9}–1.0×10^{-5}	2.0×10^{-9}	[25]
Tyr/MWNTs-CoPc-SF/GCE	Amperometry	5.0×10^{-8}–3.0×10^{-6}	3.0×10^{-8}	[21]
GR/Au-Tyr-CS/GCE	DPV	2.5×10^{-9}–3.0×10^{-6}	1.0×10^{-9}	[11]
SH-BPA/AuNPs/PCR	Piezoelectric biosensor	1.0×10^{-9}–3.5×10^{-8}	2.9×10^{-9}	[45]
MMIN/CPE	CV	6.0×10^{-7}–1.0×10^{-4}	1.0×10^{-7}	[46]
Poly(Jug-co-JugBPA)/GCE	SWV	5.0×10^{-11}–5.0×10^{-5}	1.0×10^{-11}	[47]
GS-peptide/tyrosinase/GCE	Amperometry	2.0×10^{-9}–5.5×10^{-6}	7.2×10^{-10}	[17]
Aptamer/AuNPs-GR /GCE	DPV	1.0×10^{-8}–1.0×10^{-5}	5.0×10^{-9}	[26]
Peptide/gold electrode	DPV	1.0×10^{-9}–5.0×10^{-6}	7.0×10^{-10}	[31]
Aptamer/NPGF/GCE	DPV	1.0×10^{-10}–1.0×10^{-7}	5.6×10^{-11}	This work

Note: G-MN202: graphene-hypercrosslinked resin MN202; N-GS: nitrogen-doped graphene sheets; PGA: polyglutamate acid; CNT: carbon nanotube; Arg-G: arginine functionalized graphene; PPILF: porous polymerized ionic liquid film; rGO-Fc-NH_2: reduced graphene oxide-ferrocene derivative hybrid; AuNPs: gold nanoparticles; Tyr: tyrosinase; MWNTs-CoPc-SF: multiwalled carbon nanotubes-cobalt phthalocyanine-silk fibroin film; GR/Au-Tyr-CS: graphene/gold-tyrosinase-chitosan nanocomposite; SH-BPA: thiol-labeled long chain hydrocarbon-BPA conjugate; PCR: piezoelectric ceramic resonator; MMIN/CPE: magnetic molecularly imprinted nanoparticles-based carbon paste electrode; GS: graphene-silk; AuNPs-GR: gold nanoparticles dotted graphene.

Table 2
Detection of BPA in five-time diluted human serum samples.

Samples	Spiked level (nM)	Detected level (nM)	Original level (nM)	Recovery (%)	RSD (%, $n = 3$)
1	0.5	0.53	0.029	100.2	2.14
2	1.0	1.03	0.029	100.1	4.06
3	5.0	5.07	0.029	100.8	2.47
4	10	9.92	0.029	98.9	1.62
5	50	51.17	0.029	102.3	4.53

3.6. Selectivity, reproducibility, and stability

To study the selectivity of the sensor, experiments were conducted using the chemicals with the similar structure and functional groups as BPA, such as phenol, hydroquinone, 4,4′-dihydroxybiphenyl, and bisphenol B. The aptamer/NPGF/GCE sensors were used to detect 100.0 nM each above chemicals and 10.0 nM BPA, respectively. Fig. 6 represents the DPVs corresponding to the detected chemicals. For phenol, hydroquinone, 4,4′-dihydroxybiphenyl, and bisphenol B, the developed sensor did not show observable redox peak. In contrast, the sensor exhibited a clear oxidation peak when 10.0 nM BPA was detected. Such a good selectivity of the developed sensor for BPA was attributed to the excellent specificity of the used aptamer.

To investigate the reproducibility of the developed sensor, a fresh batch of five sensors was prepared in the same way, and then was used to detect 10.0 nM BPA. The sensors achieved a relative standard deviation (RSD) of 6.2% with respect to each sensor, indicating good electrode-to-electrode reproducibility.

The stability of the developed sensor was investigated by recording the sensor response towards the same concentration of BPA with increasing time interval. First, a passel of aptamer/NPGF/GCE sensor was prepared in the same way. Then, three freshly prepared sensors of them were used to detect 10.0 nM BPA and the average value of their responses was used as the primary response. The rest sensors were stored at 4 °C and subsequently used to detect the same concentration of BPA with a time interval of ten days. The responses of the remaining sensors did not show significant change up to two months, indicating the satisfying stability of the fabricated sensor. The good stability of the developed aptamer/NPGF/GCE sensor benefits from the inherent chemical stability of NPGF and aptamer (compared with antibody recognizer), as well as the strong interaction between them through S—Au bond.

3.7. Real sample analysis

Finally, the analytical utility of the developed aptamer/NPGF/GCE sensor for practical application was explored. In most previous reports, tap water and plastic were chosen as the real samples for BPA analysis. The determination of BPA in human serum, which is of direct significance for controlling the harmful effect of BPA on human health, however, has been rarely investigated. In this work, detection of BPA in human serum samples with the developed aptamer/NPGF/GCE sensor was performed and evaluated with DPVs. The related results were listed in Table 2. The linear dependencies of spiked BPA analysis yielded an equation of I_p (μA) = (0.029 ± 0.007) + (0.997 ± 0.007) [BPA] (nM) with a correlation coefficient of 0.998 (Fig. S3 in Supporting information). According to the standard addition method, the original BPA concentration in the diluted serum sample was determined to be 0.029 nM. Taking the dilution times (five times) into consideration, the BPA concentration in the original serum sample was calculated to be 0.145 nM. The recovery of the spiked BPA was between 98.9% and 102.3% with a RSD less than 5%. These results clearly indicate the potentiality of the developed aptamer sensor for clinical detection of BPA in human serum sample.

4. Conclusions

In this work, a high performance NPGF-based aptamer sensor was developed for direct electrochemical detection of BPA. The developed sensor exhibited a detection limit of 0.056 ± 0.004 nM BPA, which was lower than the most previous reports. The sensor also showed good selectivity to BPA and long-term stability. In addition, the sensor was successfully applied for BPA detection in human serum samples, suggesting the promising potential for clinical diagnosis. The outstanding performance of the sensor is attributed to the perfect combination of NPGF with aptamer, which also demonstrates that NPGF is a promising material for bioanalysis due to its excellent catalytic property, high electroconductivity, biocompatibility, and chemical stability. Bioanalysis based on such kind of nanoporous metal materials is worth further exploring.

Acknowledgements

This work was supported by the National Science Foundation of China (21305077), Research Award Fund for Outstanding Middle-aged and Young Scientist of Shandong Province (BS2013SW031), China Postdoctoral Science Foundation (2013M531585), and Independent Innovation Foundation of Shandong University (2012HW004). The authors would like to thank Prof. Yi Ding for valuable discussion and providing essential experimental materials and facilities.

Appendix A. Supplementary data

Supplementary data associated with this article can be found, in the online version, at http://dx.doi.org/10.1016/j.aca.2015.05.002.

References

[1] D.S. Lim, S.J. Kwack, K.B. Kim, H.S. Kim, B.M. Lee, Potential risk of bisphenol amigration from polycarbonate containers after heating boiling, and microwaving, J. Toxicol. Environ. Health A 72 (2009) 1285–1291.
[2] A.V. Krishnan, P. Stathis, S.F. Permuth, L. Tokes, D. Feldman, Bisphenol-A: an estrogenic substance is released from polycarbonate flasks during autoclaving, Endocrinology 132 (1993) 2279–2286.
[3] L.N. Vandenberg, M.V. Maffini, C. Sonnenschein, B.S. Rubin, A.M. Soto, Bisphenol-A and the great divide: a review of controversies in the field of endocrine disruption, Endocr. Rev. 30 (2009) 75–95.
[4] Z. Zhang, S.M. Rhind, C. Kerr, M. Osprey, C.E. Kyle, Selective pressurized liquid extraction of estrogenic compounds in soil and analysis by gas chromatography–mass spectrometry, Anal. Chim. Acta 685 (2011) 29–35.
[5] C. Fang, N.M. Bandaru, A.V. Ellis, N.H. Voelcker, Beta-cyclodextrin decorated nanostructured SERS substrates facilitate selective detection of endocrine disruptor chemicals, Biosens. Bioelectron. 42 (2013) 632–639.
[6] V. Pacakova, L. Loukotkova, Z. Bosakova, K. Stulik, Analysis for estrogens as environmental pollutants—a review, J. Sep. Sci. 32 (2009) 867–882.
[7] J.T. Wolstenholme, E.F. Rissman, J.J. Connelly, The role of bisphenol A in shaping the brain, epigenome and behavior, Horm. Behav. 59 (2011) 296–305.

[8] A.P. Tharp, M.V. Maffini, P.A. Hunt, C.A. VandeVoort, C. Sonnenschein, A.M. Soto, Bisphenol A alters the development of the rhesus monkey mammary gland, Proc. Natl. Acad. Sci. 109 (2012) 8190–8195.
[9] K.V. Ragavan, N.K. Rastogi, M.S. Thakur, Sensors and biosensors for analysis of bisphenol-A, Trends Anal. Chem. 52 (2013) 248–260.
[10] A. Ballesteros-Gomez, S. Rubio, D. Perez-Bendito, Analytical methods for the determination of bisphenol A in food, J. Chromatogr. A 1216 (2009) 449–469.
[11] D. Pan, Y. Gu, H. Lan, Y. Sun, H. Gao, Functional graphene–gold nano-composite fabricated electrochemical biosensor for direct and rapid detection of bisphenol A, Anal. Chim. Acta 853 (2015) 297–302.
[12] M.C. Estevez, R. Galve, F. Sanchez-Baeza, M.P. Marco, Direct competitive enzyme-linked immunosorbent assay for the determination of the highly polar short-chain sulfophenyl carboxylates, Anal. Chem. 77 (2005) 5283–5293.
[13] K.V. Ragavan, L.S. Selvakumar, M.S. Thakur, Functionalized aptamers as nano-bioprobes for ultrasensitive detection of bisphenol-A, Chem. Commun. 49 (2013) 5960–5962.
[14] J.Q. Xue, D.W. Li, L.L. Qu, Y.T. Long, Surface-imprinted core–shell Au nanoparticles for selective detection of bisphenol A based on surface-enhanced Raman scattering, Anal. Chim. Acta 777 (2013) 57–62.
[15] E. Chung, J. Jeon, J. Yu, C. Lee, J. Choo, Surface-enhanced Raman scattering aptasensor for ultrasensitive trace analysis of bisphenol A, Biosens. Bioelectron. 64 (2015) 560–565.
[16] Z. Mei, H. Chu, W. Chen, F. Xue, J. Liu, H. Xu, R. Zhang, L. Zheng, Ultrasensitive one-step rapid visual detection of bisphenol A in water samples by label-free aptasensor, Biosens. Bioelectron. 39 (2013) 26–30.
[17] Y. Qu, M. Ma, Z. Wang, G. Zhan, B. Li, X. Wang, H. Fang, H. Zhang, C. Li, Sensitive amperometric biosensor for phenolic compounds based on graphene–silk peptide/tyrosinase composite nanointerface, Biosens. Bioelectron. 44 (2013) 85–88.
[18] L. Yang, H. Zhao, S. Fan, B. Li, C.P. Li, A highly sensitive electrochemical sensor for simultaneous determination of hydroquinone and bisphenol A based on the ultrafine Pd nanoparticle@TiO_2 functionalized SiC, Anal. Chim. Acta 852 (2014) 28–36.
[19] H. Yin, Y. Zhou, S. Ai, Q. Chen, X. Zhu, X. Liu, L. Zhu, Sensitivity and selectivity determination of BPA in real water samples using PAMAM dendrimer and CoTe quantum dots modified glassy carbon electrode, J. Hazard. Mater. 174 (2010) 236–243.
[20] Y. Lin, K. Liu, C. Liu, L. Yin, Q. Kang, L. Li, B. Li, Electrochemical sensing of bisphenol A based on polyglutamicacid/amino-functionalised carbon nanotubes nano composite, Electrochim. Acta 133 (2014) 492–500.
[21] H. Yin, Y. Zhou, J. Xu, S. Ai, L. Cui, L. Zhu, Amperometric biosensor based on tyrosinase immobilized onto multiwalled carbon nanotubes-cobalt phthalocyanine-silk fibroin film and its application to determine bisphenol A, Anal. Chim. Acta 659 (2010) 144.
[22] Y. Zhang, L. Wang, D. Lu, X. Shi, C. Wang, X. Duan, Sensitive determination of bisphenol A base on arginine functionalized nanocomposite graphene film, Electrochim. Acta 80 (2012) 77–83.
[23] W. Zhou, C. Sun, Y. Zhou, X. Yang, W. Yang, A facial electrochemical approach to determinate bisphenol A based on graphene-hypercross linked resin MN202 composite, Food Chem. 158 (2014) 81–87.
[24] H.X. Fan, Y. Li, D. Wu, H.M. Ma, K.X. Mao, D.W. Fan, B. Du, H. Li, Q. Wei, Electrochemical bisphenol A sensor based on N-doped graphene sheets, Anal. Chim. Acta 711 (2012) 24–28.
[25] N. Huang, M.L. Liu, H.T. Li, Y.Y. Zhang, S.Z. Yao, Synergetic signal amplification based on electrochemical reduced graphene oxide-ferrocene derivative hybrid and gold nanoparticles as an ultra-sensitive detection platform for bisphenol A, Anal. Chim. Acta 853 (2015) 249–257.
[26] L. Zhou, J. Wang, D. Li, Y. Li, An electrochemical aptasensor based on gold nanoparticles dotted graphene modified glassy carbon electrode for label-free detection of bisphenol A in milk samples, Food Chem. 162 (2014) 34–40.
[27] C. Hou, W.X. Tang, C. Zhang, Y.F. Wang, N.N. Zhu, A novel and sensitive electrochemical sensor for bisphenol A determination based on carbon black supporting ferroferric oxide nanoparticles, Electrochim. Acta 144 (2014) 324–331.
[28] M.A. Rahman, M.J.A. Shiddiky, J.-S. Park, Y.-B. Shim, An impedimetric immunosensor for the label-free detection of bisphenol A, Biosens. Bioelectron. 22 (2007) 2464–2470.
[29] B. Kang, J.H. Kim, S. Kim, K.-H. Yoo, Aptamer-modified anodized aluminum oxide-based capacitive sensor for the detection of bisphenol A, Appl. Phys. Lett. 98 (2011) 073703.
[30] S. Song, L. Wang, J. Li, J. Zhao, C. Fan, Aptamer-based biosensors, Trends Anal. Chem. 27 (2008) 108–117.
[31] J. Yang, S.E. Kim, M. Cho, I.K. Yoo, W.S. Choe, Y. Lee, Highly sensitive and selective determination of bisphenol-A using peptide-modified gold electrode, Biosens. Bioelectron. 61 (2014) 38–44.
[32] Z.C. Sanchez-Acevedo, J. Riu, F.X. Rius, Fast picomolar selective detection of bisphenol A in water using a carbon nanotube field effect transistor functionalized with estrogen receptor-alpha, Biosens. Bioelectron. 24 (2009) 2842–2846.
[33] Y. Ding, Y.J. Kim, J. Erlebacher, Nanoporous gold leaf: ancient technology/advanced material, Adv. Mater. 16 (2004) 1897–1900.
[34] Y. Ding, M. Chen, Nanoporous metals for catalytic and optical applications, MRS Bull. 34 (2009) 569–576.
[35] X. Zhang, Y. Ding, Unsupported nanoporous gold for heterogeneous catalysis, Catal. Sci. Technol. 3 (2013) 2862–2868.
[36] J. Zhang, P. Liu, H. Ma, Y. Ding, Nanostructured porous gold for methanol electro-oxidation, J. Phys. Chem. C 111 (2007) 10382–10388.
[37] Z. Liu, J. Du, C. Qiu, L. Huang, H. Ma, D. Shen, Y. Ding, Electrochemical sensor for detection of *p*-nitrophenol based on nanoporous gold, Electrochem. Commun. 11 (2009) 1365–1368.
[38] M. Jo, J.Y. Ahn, J. Lee, S. Lee, S.W. Hong, J.W. Yoo, J. Kang, P. Dua, D. Lee, S. Hong, S. Kim, Development of single-stranded DNA aptamers for specific bisphenol A detection, Oligonucleotides 21 (2011) 85–91.
[39] E. Mazzotta, C. Malitesta, E. Margapoti, Direct electrochemical detection of bisphenol A at PEDOT-modified glassy carbon electrodes, Anal. Bioanal. Chem. 405 (2013) 3587–3592.
[40] M. Ma, X. Tu, G. Zhan, C. Li, S. Zhang, Electrochemical sensor for bisphenol A based on a nanoporous polymerized ionic liquid interface, Microchim. Acta 181 (2014) 565–572.
[41] P. Chandra, H.B. Noh, M.S. Won, Y.B. Shim, Detection of daunomycin using phosphatidylserine and aptamer co-immobilized on Au nanoparticles deposited conducting polymer, Biosens. Bioelectron. 26 (2011) 4442–4449.
[42] T.M. Herne, M.J. Tarlov, Characterization of DNA probes immobilized on gold surfaces, J. Am. Chem. Soc. 119 (1997) 8916–8920.
[43] A.J. Bard, L.R. Faulkner, Electrochemical Methods: Fundamentals and Applications, Wiley, New York, 1980.
[44] E. Laviron, General expression of the linear potential sweep voltammogram in the case of diffusionless electrochemical systems, J. Electroanal. Chem. 101 (1979) 19–28.
[45] L. Hu, C.C. Fong, L. Zou, W.L. Wong, K.Y. Wong, R.S.S. Wu, M. Yang, Label-free detection of endocrine disrupting chemicals by integrating a competitive binding assay with a piezoelectric ceramic resonator, Biosens. Bioelectron. 53 (2014) 406–413.
[46] L. Zhu, Y. Cao, G. Cao, Electrochemical sensor based on magnetic molecularly imprinted nanoparticles at surfactant modified magnetic electrode for determination of bisphenol A, Biosens. Bioelectron. 54 (2014) 258–261.
[47] X. Wang, S. Reisberg, N. Serradji, G. Anquetin, M.C. Pham, W. Wu, C.Z. Dong, B. Piro, E-assay concept: detection of bisphenol A with a label-free electrochemical competitive immunoassay, Biosens. Bioelectron. 53 (2014) 214–219.